Biosensors and Bioelectronics 150 (2020) 111958

Contents lists available at ScienceDirect

Biosensors and Bioelectronics

journal homepage: http://www.elsevier.com/locate/bios

# Peptide cleavage-mediated photoelectrochemical signal on-off via CuS electronic extinguisher for PSA detection

Jinge Zhao [a,1], Shaopeng Wang [a,1], Sibao Zhang [b], Peini Zhao [d], Jianrong Wang [c,**], Mei Yan [d], Shenguang Ge [a,*], Jinghua Yu [d]

[a] Shandong Collaborative Innovation Center of Technology and Equipments for Biological Diagnosis and Therapy, Institute for Advanced Interdisciplinary Research, University of Jinan, Jinan, 250022, PR China
[b] Chemical Technology Academy of Shandong Province, Qingdao University of Science and Technology, Jinan, 250014, PR China
[c] School of Materials Science and Engineering, University of Jinan, Jinan, 250022, PR China
[d] School of Chemistry and Chemical Engineering, University of Jinan, Jinan, 250022, PR China

ARTICLE INFO

*Keywords:*
Photoelectrochemical sensor
Peptide
Prostate specific antigen
$TiO_2$ nanotubes

In this work, a peptide-based photoelectrochemical (PEC) biosensor was constructed based on CdTe/$TiO_2$ sensitized structure as electrode and CuS nanocrystals as signal amplifier for the ultrasensitive detection of protein. After peptide was fixed to the CdTe/$TiO_2$ electrode surface, the double-helix DNA (dsDNA) was immobilized at the end of the peptide and used as a carrier to immobilize the doxorubicin-copper sulfide nanocrystals (Dox-CuS) conjugates. As a proof of concept, prostate specific antigen (PSA) has been chosen as the model. In absence of PSA, CuS nanocrystals could consume electron donors and exciting light energy. Additionally, the steric hindrance effect of biomacromolecules hindered the movement of electron donors to the photoelectrode. Eventually, the photoelectric response signal was reduced, and the biosensor was in a "signal off" state. When PSA existed, the PSA specifically cleaved the peptide, and DNA/Dox-CuS probes were released from the electrode surface, resulting in a "signal on" state. The PEC biosensor revealed good specificity, stability, and reproducibility, and it exhibited excellent application in PSA analysis with a linear range from 0.005 to 20 ng $mL^{-1}$ and a low detection limit of 0.0015 ng $mL^{-1}$. This PEC biosensor may have potential applications in bioanalysis, disease diagnostics, and clinical biomedicine.

## 1. Introduction

Peptide-based biosensors can convert undetectable changes caused by binding activity between peptides and target analytes into detectable signals (Liu et al., 2015). The high specificity, long-term stability of peptide makes it more useful in the construction of various biosensing platforms, such as peptide-based electrochemical biosensors (Lee et al., 2017; Zheng et al., 2018), optical biosensors (Zhang et al., 2017) and electrochemical luminescence biosensors (Oh et al., 2007). With the presence of the target, the constructive of the peptides undergoes changes, such as the peptide's stretching, bending, or breaking. And some peptide-based biosensors are established to detect proteins based on target-induced peptide separation strategy, such as tryptase (Wu et al., 2018), caspase-3 (Yang et al., 2018) and prostate specific antigen (Cai et al., 2018; Qi et al., 2014). After the peptides are cleaved, the markers modified at the end of peptides break away from the biosensors, resulting in an increased or decreased signal. Although a variety of peptide-based biosensors have been proposed in recent years, there is still a need to develop a simple, multifunctional and efficient peptide-based biosensor to detect targets.

Photoelectrochemical (PEC) biosensor with low background signal has attracted more and more researchers' attention because of its simple equipment, low cost and easy miniaturization (Ge et al., 2016; Qiu et al., 2018; Ye et al., 2016; Zhang et al., 2016). In the PEC sensing system, it is necessary to exploit photoelectrochemical materials with wider light absorption range and higher photocurrent conversion efficiency, especially $TiO_2$-based composites (Chu et al., 2019; Li et al., 2018; Zhu et al., 2017). The large band gap of $TiO_2$ leads to low utilization of light energy and limits its direct application (Liu et al., 2017; Tian et al., 2012). In order to construct a strong initial PEC signal by $TiO_2$-based composites,

* Corresponding author.
** Corresponding author.
*E-mail addresses:* mse_wangjr@ujn.edu.cn (J. Wang), chm_gesg@163.com (S. Ge).
[1] These authors contributed equally to this work.

https://doi.org/10.1016/j.bios.2019.111958
Received 16 June 2019; Received in revised form 28 November 2019; Accepted 6 December 2019
Available online 9 December 2019

non-metallic elements (Hu et al., 2016; Zhang et al., 2013), metal nanoparticles (Hao et al., 2018; Su et al., 2013) and narrow band gap semiconductors (Schneider et al., 2014; Seabold et al., 2008; Zhu et al., 2014a) are doped into the interior of $TiO_2$ or loaded onto the $TiO_2$ surface, such as $TiO_2/MoO_3$ (Pang et al., 2017) and $TiO_2$/CdSeTe/CdS: Mn (Fan et al., 2016) structures. In addition, CuS nanocrystals are usually introduced into the sensor as signal quenchers. Under illumination, CuS nanocrystals are capable of producing photogenerated electrons that are trapped by dissolved oxygen while consuming electron donors (Hsu et al., 2014), resulting in low photocurrent signal.

Herein, using CuS NCs as a signal amplification element, a peptide-based photoelectrochemical biosensor was constructed based on the reaction that the prostate specific antigen (PSA) was capable of cleaving a specific amino acid sequence (Denmeade et al., 1997; Parnsubsakul et al., 2017; Wu et al., 2016), as shown in Scheme 1. Ordered $TiO_2$ nanotubes array was obtained on a high purity titanium plate by anodization. Then the CdTe QDs film was immobilized on the surface of the obtained $TiO_2$-NTs, and the formed composite structure had a high photocurrent response signal. After that, the peptide was linked to the CdTe/$TiO_2$ electrode through an amide bond between the amino group of the peptide and the carbonyl group of the CdTe quantum dot. Subsequently, R1, R2, H1 and H2 were sequentially fixed on the surface of the electrode to form dsDNA. At last, CuS NCs was efficiently immobilized on dsDNA via Dox inserting into the dsDNA. Before the PSA was incubated with the sensor, the electron donor and radiant light were consumed by CuS NCs, and the steric hindrance effect of non-conductive substances such as peptides and DNA, leading to the photocurrent intensity of the sensor was low. When the PSA was incubated with the sensor, the photocurrent intensity evidently increased due to the partial release of CuS-Dox/DNA/peptide from the electrode surface. As a signal switch, the PSA controlled the transition of the sensor state from "signal off" to "signal on". In this work, a PEC biosensor with high sensitivity and selectivity was successfully fabricated for PSA detection. In addition, a general method based on peptides and CuS NCs was developed for the design of PEC biosensors to detect other important proteins.

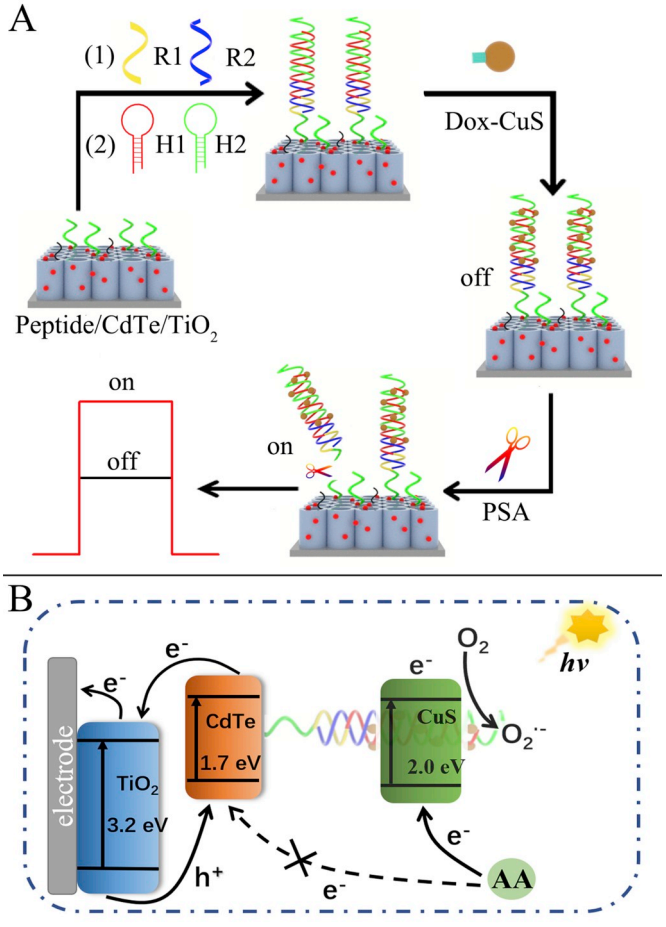


**Scheme 1.** Schematic Diagram of the Construction (A) and the Response Mechanism (B) of PEC biosensor.

## 2. Experimental section

### 2.1. Synthesis of $TiO_2$ nanotubes

$TiO_2$-NTs were obtained by anodic oxidation of a pure titanium sheet. Before the anodization, Ti sheets were ultrasonically cleaned sequentially with acetone, ethanol and deionized (DI) water for 10 min. Then the cleaned titanium sheet was dried and anodized at 40 V in ethylene glycol solution containing 1 vol % water and 0.35 wt % $NH_4F$ for 2 h. A constant voltage power supply was used to provide a stable voltage with a graphite as the cathode in this anodizing system. The anodized Ti sheets were washed with DI water and dried in air. Finally, the Ti sheets were annealed at 450 °C for 2 h in air atmosphere in order to form the highly ordered and uniform anatase $TiO_2$-NTs. The $TiO_2$-NTs were obtained after cooling to room temperature.

### 2.2. Synthesis of CdTe QDs

The synthetic method of CdTe QDs was based on previous report with some modifications (Fan et al., 2014). And detailed procedures were described in the supplementary material.

### 2.3. Synthesis of CuS NCs and Dox-CuS conjugates

CuS NCs and Dox-CuS conjugates were synthesized according to the reported method in the literature (Zhu et al., 2014b). And detailed procedures were described in the supplementary material.

### 2.4. Fabrication of sensor

Firstly, the surface of the $TiO_2$-NTs electrode was modified with CdTe QDs through a simple layer by layer assembly method. In detail, the $TiO_2$-NTs electrode was alternately immersed in 1% PDDA solution and CdTe QDs solution for 10 min, washed with DI water after each dipping process. After repeating the above process four times, the CdTe/$TiO_2$ electrode was obtained. A 50 μL aliquot of the peptide solution containing EDC (1 mg) and NHS (0.5 mg) was dropped onto the prepared CdTe/$TiO_2$ electrode and kept at 4 °C for 8 h, followed by washing with PBS and blocking with 1 mM MCH for 2 h. Then, 50 μL R1 (1 μM) DNA solution containing EDC (1 mg) and NHS (0.5 mg) was added to electrode and kept at 4 °C overnight. Next, 50 μL R2 (1 μM) DNA solution was dropped onto the surface of the prepared electrode for 1 h. After that, the electrode was rinsed with PBS and incubated with a mixture solution containing hairpin probe H1 (1 μM) and hairpin probe H2 (1 μM) for 2 h. Finally, the modified electrode was immersed in Dox-CuS solution and kept at 4 °C for 7 h. Each process of the modifications was characterized by EIS and photocurrent signal, and the sensor construction process is shown in Scheme 1A.

## 3. Results and discussion

### 3.1. Materials characterization

Fig. 1A showed the SEM image of the surface and the cross-sectional of $TiO_2$-NTs. According to the image, the highly ordered, uniform-sized $TiO_2$-NTs grown on Ti sheet have been obtained. The nanotubes had an average pore size of about 60 nm, a wall thickness of about 17 nm and a nanotube length of about 3 μm. Fig. 1B showed the XRD patterns of

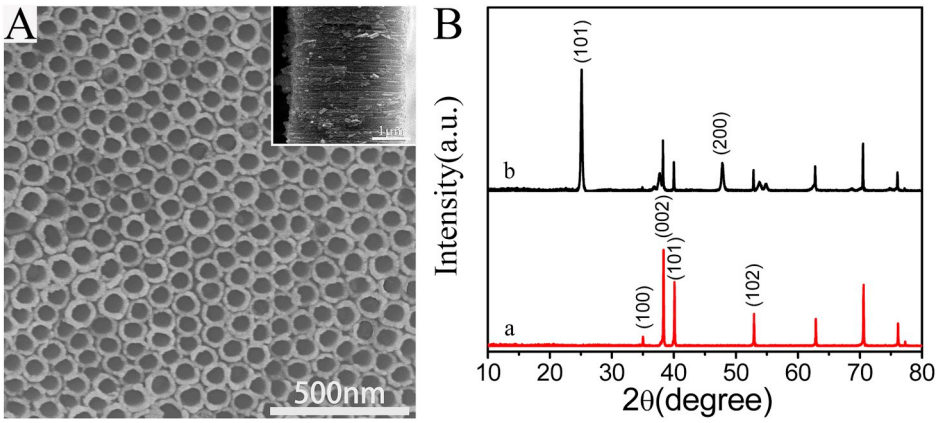


**Fig. 1.** (A) SEM images of the $TiO_2$-NTs. The inset shows the cross-sectional SEM image of $TiO_2$-NTs. (B) XRD spectra of (a) Ti sheet and (b) $TiO_2$-NTs grown on Ti sheet.

blank Ti sheet and $TiO_2$-NTs. The position of the main diffraction peaks of the Ti sheet were at $2\theta = 35.1^\circ$, $38.3^\circ$, $40.1^\circ$, $52.9^\circ$ (curve a), correspond to (100), (002), (101), and (102) crystalline planes of the hexagonal phase of metallic Ti (JCPDS no. 44–1294), respectively. In curve b, two peaks at $2\theta = 25.2^\circ$ and $48.2^\circ$ correspond to the tetragonal phase of anatase $TiO_2$ (101) and (200) facets (JCPDS no 21–1272) (Gong et al., 2011), respectively. This proved that $TiO_2$-NTs had been formed on the Ti substrate. Therefore, SEM and XRD results indicated that the uniform $TiO_2$-NTs electrode was successfully fabricated.

Fig. 2A and B showed the transmission electron microscopy (TEM) image and UV–vis absorption spectrum of the synthesized MPA-capped CdTe QDs, respectively. The average size of CdTe QDs was about 4.0 nm as shown in Fig. 2A. As Fig. 2B illustrated, the absorption edge and the evident absorption peak of the CdTe QDs were located at 700 nm and 635 nm, respectively. According to Peng's empirical equations (Yu et al., 2003), the diameter of the CdTe QDs was estimated to be 4.07 nm, which was in good agreement with the data observed by TEM.

Fig. 2C and D showed the TEM image of CuS NCs and the UV–vis absorption spectra of the CuS NCs, Dox and Dox-CuS compounds, respectively. As showed in Fig. 2C, the synthesized CuS NCs were spherical particles with a relatively uniform morphology and an average diameter of 5 nm. The CuS NCs have a strong absorption in the short wavelength region (Fig. 2D curve a). Compared with the bulk CuS, the short-wavelength absorption margin of the CuS NCs was about 600 nm with a significant blue shift. UV–vis spectra proved that CuS NCs were successfully synthesized. Meanwhile, the UV–vis absorption spectra

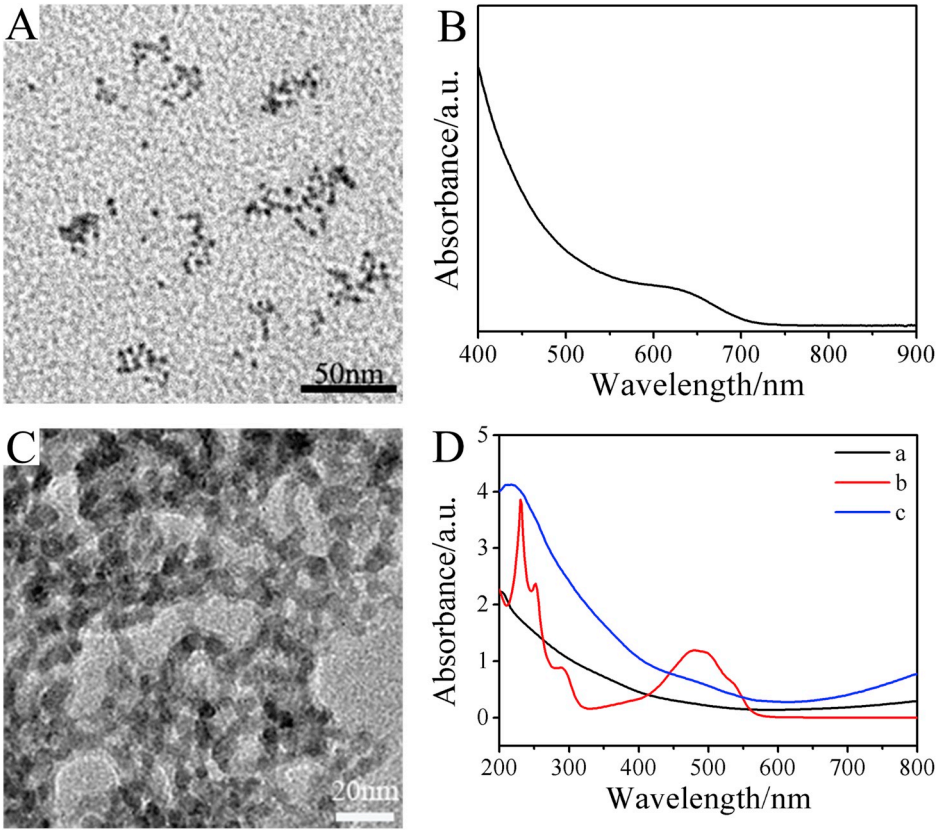


**Fig. 2.** (A) TEM image and (B) UV–vis absorption spectra of CdTe QDs, (C) TEM image of CuS NCs and (D) UV–vis absorption spectra of (a) CuS NCs, (b) Dox and (c) Dox-CuS compounds.

were also used to confirm the synthesis of Dox-CuS compounds. Dox had a characteristic absorption peak at 480 nm (curve b), and the absorption spectrum of the Dox-CuS compounds showed that the absorption increased near 480 nm (curve c). Furthermore, in the Dox-CuS compounds, the absorption peak disappeared at 230 nm and an absorption peak appeared at 215 nm because the $-NH_2$ group was consumed and formed the amide bond with a carboxyl group. The results indicated that the Dox-CuS compounds had been successfully synthesized.

### 3.2. PEC mechanism analysis

The PEC mechanism of biosensor is showed in Scheme 1B. The CdTe/$TiO_2$-NTs sensitized structure obtained by using $TiO_2$-NTs array as the substrate for the deposition of CdTe QDs improved photoelectric conversion efficiency. On one hand, narrow band gap semiconductor CdTe QDs (1.5eV) broadened the absorption range of the sensitized structure for light, resulting in efficiently harnessing of visible light. On the other hand, the existence of band alignment between $TiO_2$-NTs and CdTe QDs effectively promoted rapid transfer of electrons, which was beneficial for inhibiting the recombination of electron-hole pairs (Jang et al., 2015; Tang et al., 2014; Wang et al., 2016). This mechanism was confirmed by comparing the photocurrent signal of CdTe/$TiO_2$-NTs electrode and the blank $TiO_2$-NTs electrode.

DNA/Dox-CuS conjugates were an important part of the biosensor for increasing photocurrent response. The biomolecular portion of the DNA/Dox-CuS conjugates with significant steric hindrance hindered electron transfer, resulting in the photocurrent intensity decreased obviously. More importantly, CuS NCs were used as signal-off unit based on two main factors. Firstly, the broad absorption range of the prepared CuS NCs partially overlapped the absorption ranges of CdTe QD and $TiO_2$-NTs, which leaded to less light reaching the CdTe/$TiO_2$ electrode surface and weakened photoelectrochemical response. Secondly, CuS NCs generated electron-hole pairs under photoexcitation. The holes were neutralized by the AA while the photogenerated electrons were trapped by $O_2$ dissolved in solution to form $O_2^{\bullet-}$. The above reactions of CuS NCs resulted in the decreased photocurrent intensity in the presence of AA which supplied electrons to holes generated in the sensitized structure of CdTe/$TiO_2$-NTs. The PEC response signals were tested under three different conditions to prove that dsDNA could effectively immobilize Dox-CuS NCs conjugates (Fig. S1). In addition, Fig. S3 showed the experiment about PSA cleaving peptide.

Concisely, the CdTe/$TiO_2$-NTs sensitization electrode could effectively heighten photocurrent response, and the DNA/Dox-CuS conjugates as signal-off unit could effectively decrease photocurrent intensity.

### 3.3. Electrochemical behavior of the stepwise process

In this strategy, the assembly process of the sensor was characterized by electrochemical impedance spectroscopy (EIS) (Sun et al., 2018). Fig. 3A showed the impedance spectra at different stages of the electrode fabrication process. The impedance spectra showed a semicircle controlled by electron transfer in the high frequency region and a straight line controlled by diffusion in the low frequency region. The semicircular diameter of the EIS spectra indicates the electron transfer resistance (Ret) value of the $[Fe(CN)_6]^{3-/4-}$ redox system. For the blank $TiO_2$-NTs electrode, there was a small Ret value about 1332 Ω (curve a). After CdTe QDs were coated on the surface of $TiO_2$-NTs electrode layer by layer, the Ret value gradually increased to 1600 Ω (curve b), due to the PDDA/CdTe QDs film impeded the redox probe from entering the electrode surface. The Ret continuously increased to 2053 Ω (curve c) after peptide and MCH were successively assembled on the electrode, which could be attributed to the steric hindrance effect of peptide and MCH. After the DNA was fixed on the obtained electrode, the Ret value evidently increased to 3048 Ω (curve d), which was because the steric hindrance effect of double-stranded DNA could increase the Ret. After the Dox-CuS NCs dropped on the electrode and incubated for a while, the Ret value increased to 3762 Ω (curve e). Additionally, the Ret value of the resulting electrode dramatically decreased to 2138 Ω after incubation with PSA (curve f). The decrement of Ret value was mainly attributed to the leaving of partial peptide and DNA/Dox-CuS after the PSA cut off the peptide. Therefore, the successful construction of PEC biosensor could be proved by the reasonable change of EIS.

### 3.4. PEC behaviors of the modified electrode

The alteration of photocurrent signal intensity could monitor the stepwise building process of the biosensor and validate the feasibility of PEC biosensor for protein analysis (Fig. 3B). The $TiO_2$-NTs electrode with wide band gap showed a photocurrent signal (curve a) about 0.9 mA in PBS containing 0.1 M AA. After CdTe QDs was deposited on $TiO_2$-NTs electrode, further increased intensity (curve b) about 2.2 mA was observed. The photocurrent response of the CdTe/$TiO_2$ electrode was nearly three times stronger than that of the blank $TiO_2$-NTs electrode. This indicated that the CdTe QDs had been successfully loaded on the $TiO_2$-NTs electrode and the CdTe/$TiO_2$ sensitized electrode could effectively improve the photoelectric conversion efficiency. The photocurrent intensity decreased after the peptide and MCH were incubated on the surface of CdTe/$TiO_2$ electrode (curve c), because of the enhanced steric hindrance and reduced electron transfer efficiency. Subsequently, the photocurrent further decreased after the dsDNA as a carrier was attached to the peptide (curve d). The photocurrent markedly decreased to 1.32 mA as the Dox-CuS compounds dropped on the electrode (curve e). The photocurrent of the PEC biosensor conspicuously increased after incubated with PSA for some time (curve f). All of the above results also proved the successful fabrication of the PEC biosensor.

### 3.5. Evaluating the stability and specificity of the PEC biosensor

Stability and specificity are important indicators for evaluating the performance of the prepared PEC biosensor. The stability of the sensor was detected by testing the photocurrents of the CdTe/$TiO_2$-NTs

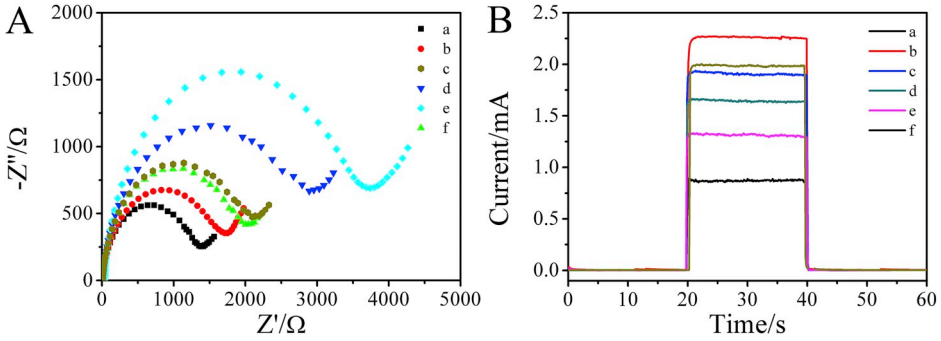


**Fig. 3.** (A) EIS of different modification process in 0.1 M KCl solution containing 5 mM (1:1) $[Fe(CN)_6]^{3-/4-}$ with the range from 0.1 Hz to $10^5$ Hz at an alternate voltage of 5 mV; (B) Photocurrent responses in PBS (0.1 M, pH 7.4) containing 0.1 M AA. (a) The $TiO_2$-NTs electrode, (b) CdTe/$TiO_2$ electrode, (c) MCH/peptide/CdTe/$TiO_2$ electrode, (d) DNA/MCH/peptide/CdTe/$TiO_2$ electrode, (e) Dox-CuS/DNA/MCH/peptide/CdTe/$TiO_2$ electrode and (f) after incubation with 100 ng $mL^{-1}$ PSA.

electrode and CuS/DNA/peptide/CdTe/$TiO_2$-NTs electrode under repeated light irradiation. As could be seen from Fig. 4A, the stability of the CdTe/$TiO_2$ electrode was studied in PBS containing AA under repeated light irradiation. The photocurrent kept almost invariable during 8 times of continuous on/off cycle irradiation. This indicated the prepared photoactive material had good reproducibility and stability for constructing a PEC biosensor. We also examined the stability of different CuS/DNA/peptide/CdTe/$TiO_2$-NTs electrodes and the electrodes at different storage time. Fig. 4B showed that the photocurrent signal fluctuation range between different electrodes was small, and the relative standard deviation (RSD) values were 2.3% and 3.1% before and after incubation of the electrodes with PSA, respectively. The prepared electrodes were kept at 4 °C and measured at different storage time. As shown in Fig. 4C, the photoelectrochemical response signal gradually decreased within 7 days. Finally, the PEC electrode could still retain 84.5% and 86.2% of the original PEC signal and the amplitude of the signal attenuation was quite slight.

The selectivity of peptide-based PEC biosensor was evaluated by comparison of the photocurrents with some interference agents, such as immunoglobulin G (IgG), carcinoembryonic antigen (CEA), casein, and alpha-fetoprotein (AFP). As showed in Fig. 4D, the PEC biosensor was incubated with interference agents and the obtained photocurrent signals were almost consistent with the background signal. In addition, the biosensor was incubated with the PSA solution containing the interference agents for 40 min. The photocurrent signal indicated that the presence of interference agents did not affect the signal intensity. According to Fig. S4, the sensor also showed good selectivity in biological samples. Thus, the photocurrent of the biosensor indicated that PSA could specifically recognize and cleave peptide.

### 3.6. Analytical performance

Under the optimum conditions (Fig. S2), the obtained PEC biosensor was used for the determination of PSA. PSA could specifically recognize and cleave peptide, which leaded to the detachment of fractional peptide and Dox-CuS/DNA probe. A good linear relationship between the photocurrent difference and the logarithm of PSA concentration from 0.005 to 20.00 ng $mL^{-1}$ was displayed (Fig. 5B). The regression equation was $\Delta I = 0.50802 + 0.1449\ \lg c_{PSA}$ (ng·$mL^{-1}$) with a correlation coefficient of 0.991. According to the formula (Çakıroğlu and Özacar, 2019), it was found that the limit of detection was 0.0015 ng $mL^{-1}$ and the limit of quantitation was 0.0047 ng $mL^{-1}$. This proposed PEC biosensor exhibited a wider linear range and lower detection than some of the other reported methods (Table S1) for PSA assays.

## 4. Conclusion

In summary, a photoelectrochemical biosensing platform based on signal amplification of Dox−CuS conjugates and synergistic effect of CdTe/$TiO_2$ sensitization structure for sensitive and selective detection of PSA was successfully fabricated. The greatly enhanced photoelectric conversion efficiency came from the effective matching of energy levels between $TiO_2$-NTs and CdTe QDs. The Dox-CuS NCs can significantly reduce the photocurrent response with the apparent steric hindrance, the competitive absorption of the excitation light and the efficient consumption of the electron donor. The dsDNA as carrier material increased the loading of Dox-CuS NCs to achieve the goal of signal amplification. According to the target-induced separation strategy, the PSA could specifically cleave the peptide, and successfully realize the signal "on-off" switching system for highly selective and sensitive detection for PSA. The proposed PEC peptide-based biosensors might be used in many fields, including biochemical analysis and clinical assays.

## Declaration of competing interest

The authors declare that they have no known competing financial interests or personal relationships that could have appeared to influence the work reported in this paper.

## CRediT authorship contribution statement

**Jinge Zhao:** Conceptualization, Methodology, Writing - original draft. **Shaopeng Wang:** Writing - review & editing, Resources. **Sibao Zhang:** Visualization, Data curation. **Peini Zhao:** Resources,

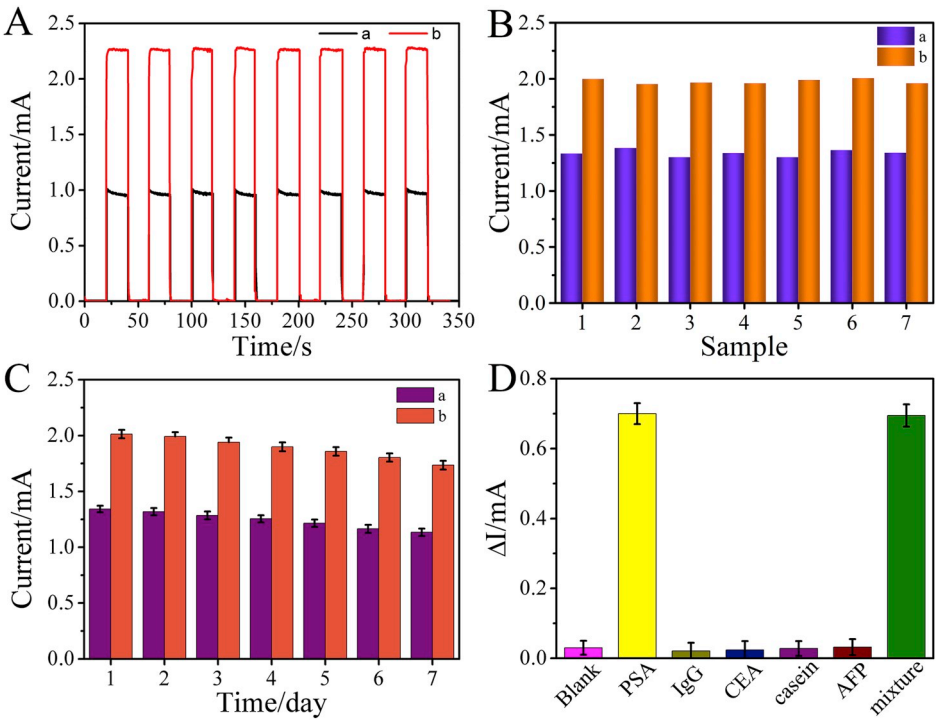


**Fig. 4.** (A) The photocurrent response of the (a) $TiO_2$-NTs electrode and (b) CdTe/$TiO_2$ electrode under repeated light irradiation. The photocurrents response of (B) different PEC biosensors and (C) the biosensor at different storage times before (a) and after (b) incubation with PSA, respectively. (D) Selectivity of the proposed biosensor for blank, PSA (100 ng·$mL^{-1}$), IgG (100 ng·$mL^{-1}$), CEA (100 ng·$mL^{-1}$), casein (100 ng·$mL^{-1}$), AFP (100 ng·$mL^{-1}$) and their mixture. All the photocurrents were measured in PBS (0.1 M pH 7.4) containing AA (0.1 M) with an applied potential of 0 V.

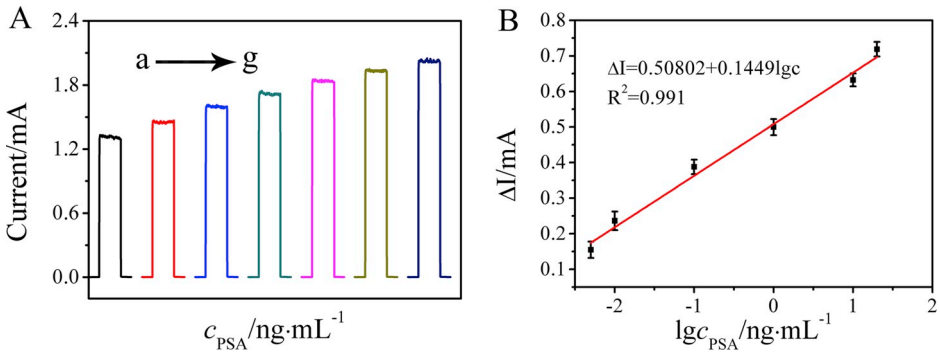


**Fig. 5.** (A) Photocurrent responses of the different concentration of PSA. The concentrations are 0, 0.005, 0.01, 0.1, 1, 10 and 20 ng mL$^{-1}$ (from a to g). (B) Dependence of $\Delta I$ on PSA concentration ($\Delta I = I - I_0$, where $I$ and $I_0$ represent the photocurrent intensity of the peptide-based PEC biosensor with or without PSA incubated, respectively).

Visualization. **Jianrong Wang:** Funding acquisition, Project administration. **Mei Yan:** Visualization, Data curation. **Shenguang Ge:** Conceptualization, Supervision, Funding acquisition. **Jinghua Yu:** Writing - review & editing, Resources.

## Acknowledgements

This work was supported by the National Natural Science Foundation of China (21775055, 21874055); Excellent Youth Innovation Team in Universities of Shandong (2019KJC016); The Project of "20 items of University" of Jinan (2018GXRC001); the Taishan Scholars program and Case-by-Case Project for Top Outstanding Talents of Jinan.

## Appendix A. Supplementary data

Supplementary data to this article can be found online at https://doi.org/10.1016/j.bios.2019.111958.

## References

Cai, G., Yu, Z., Ren, R., Tang, D., 2018. ACS Sens. 3 (3), 632–639.
Çakıroğlu, B., Özacar, M., 2019. Biosens. Bioelectron. 141, 111385.
Chu, Y., Deng, A.-P., Wang, W., Zhu, J.-J., 2019. Anal. Chem. 91 (5), 3619–3627.
Denmeade, S.R., Lou, W., Lovgren, J., Malm, J., Lilja, H., Isaacs, J.T., 1997. Cancer Res. 57 (21), 4924–4930.
Fan, G.C., Han, L., Zhang, J.R., Zhu, J.J., 2014. Anal. Chem. 86 (21), 10877–10884.
Fan, G.C., Zhu, H., Du, D., Zhang, J.R., Zhu, J.J., Lin, Y., 2016. Anal. Chem. 88 (6), 3392–3399.
Ge, S., Liang, L., Lan, F., Zhang, Y., Wang, Y., Yan, M., Yu, J., 2016. Sens. Actuators B Chem. 234, 324–331.
Gong, D., Grimes, C.A., Varghese, O.K., Hu, W., Singh, R.S., Chen, Z., Dickey, E.C., 2011. J. Mater. Res. 16 (12), 3331–3334.
Hao, N., Hua, R., Zhang, K., Lu, J., Wang, K., 2018. Anal. Chem. 90 (22), 13207–13211.
Hsu, S.-W., Ngo, C., Tao, A.R., 2014. Nano Lett. 14 (5), 2372–2380.
Hu, W., Zhou, W., Zhang, K., Zhang, X., Wang, L., Jiang, B., Tian, G., Zhao, D., Fu, H., 2016. J. Mater. Chem. A. 4 (19), 7495–7502.
Jang, H., Choi, M.H., Yim, Y., Kim, Y.K., Min, D.H., 2015. Adv. Healthc. Mater. 4 (12), 1833–1840.
Lee, J., Yun, J.Y., Lee, W.C., Choi, S., Lim, J., Jeong, H., Shin, D.-S., Park, Y.J., 2017. Sens. Actuators B Chem. 240, 735–741.
Li, L., Zheng, X., Huang, Y., Zhang, L., Cui, K., Zhang, Y., Yu, J., 2018. Anal. Chem. 90 (23), 13882–13890.
Liu, P.P., Liu, X., Huo, X.H., Tang, Y., Xu, J., Ju, H., 2017. ACS Appl. Mater. Interfaces 9 (32), 27185–27192.
Liu, Q., Wang, J., Boyd, B.J., 2015. Talanta 136, 114–127.
Oh, K.J., Cash, K.J., Hugenberg, V., Plaxco, K.W., 2007. Bioconjug. Chem. 18 (3), 607–609.
Pang, X., Bian, H., Su, M., Ren, Y., Qi, J., Ma, H., Wu, D., Hu, L., Du, B., Wei, Q., 2017. Anal. Chem. 89 (15), 7950–7957.
Parnsubsakul, A., Safitri, R.E., Rijiravanich, P., Surareungchai, W., 2017. J. Electroanal. Chem. 785, 125–130.
Qi, H., Li, M., Dong, M., Ruan, S., Gao, Q., Zhang, C., 2014. Anal. Chem. 86 (3), 1372–1379.
Qiu, Z., Shu, J., Tang, D., 2018. Anal. Chem. 90 (1), 1021–1028.
Schneider, J., Matsuoka, M., Takeuchi, M., Zhang, J., Horiuchi, Y., Anpo, M., Bahnemann, D.W., 2014. Chem. Rev. 114 (19), 9919–9986.
Seabold, J.A., Shankar, K., Wilke, R.H.T., Paulose, M., Varghese, O.K., Grimes, C.A., Choi, K.-S., 2008. Chem. Mater. 20 (16), 5266–5273.
Su, F., Wang, T., Lv, R., Zhang, J., Zhang, P., Lu, J., Gong, J., 2013. Nanoscale 5 (19), 9001–9009.
Sun, X.L., Wang, H., Jian, Y.N., Lan, F.F., Zhang, L.N., Liu, H.Y., Ge, S.G., Yu, J.H., 2018. Biosens. Bioelectron. 105, 218–225.
Tang, J., Zhang, Y., Kong, B., Wang, Y., Da, P., Li, J., Elzatahry, A.A., Zhao, D., Gong, X., Zheng, G., 2014. Nano Lett. 14 (5), 2702–2708.
Tian, C.Y., Zhao, W.W., Wang, J., Xu, J.J., Chen, H.Y., 2012. Analyst 137 (13), 3070–3075.
Wang, Q., Shi, X., Liu, E., Xu, J., Crittenden, J.C., Zhang, Y., Cong, Y., 2016. Ind. Eng. Chem. Res. 55 (17), 4897–4904.
Wu, F.F., Zhou, Y., Zhang, H., Yuan, R., Chai, Y.Q., 2018. Anal. Chem. 90 (3), 2263–2270.
Wu, M.S., Chen, R.N., Xiao, Y., Lv, Z.X., 2016. Talanta 161, 271–277.
Yang, R., Zou, K., Li, Y., Meng, L., Zhang, X., Chen, J., 2018. Anal. Chem. 90 (15), 9480–9486.
Ye, C., Wang, M.Q., Gao, Z.F., Zhang, Y., Lei, J.L., Luo, H.Q., Li, N.B., 2016. Anal. Chem. 88 (23), 11444–11449.
Yu, W.W., Qu, L., Guo, W., Peng, X., 2003. Chem. Mater. 15 (14), 2854–2860.
Zhang, L., Sun, Y., Liang, Y.-Y., He, J.-P., Zhao, W.-W., Xu, J.-J., Chen, H.-Y., 2016. Biosens. Bioelectron. 85, 930–934.
Zhang, Q., Zhang, D., Xu, G., Xu, Y., Lu, Y., Li, S., Liu, Q., 2017. Sens. Actuators B Chem. 242, 443–449.
Zhang, X., Huang, H., Liu, J., Liu, Y., Kang, Z., 2013. J. Mater. Chem. A. 1 (38), 11529.
Zheng, X., Li, L., Cui, K., Zhang, Y., Zhang, L., Ge, S., Yu, J., 2018. ACS Appl. Mater. Interfaces 10 (4), 3333–3340.
Zhu, A., Zhao, Q., Li, X., Shi, Y., 2014. ACS Appl. Mater. Interfaces 6 (1), 671–679.
Zhu, L., Lu, H., Hao, D., Wang, L., Wu, Z., Wang, L., Li, P., Ye, J., 2017. ACS Appl. Mater. Interfaces 9 (44), 38537–38544.
Zhu, Y.D., Peng, J., Jiang, L.P., Zhu, J.J., 2014. Analyst 139 (3), 649–655.